TOROS CAMERA CALIBRATION

An Undergraduate Research Scholars Thesis

by

ALEXANDRA BOONE

Submitted to the LAUNCH: Undergraduate Research office at
Texas A&M University
in partial fulfillment of the requirements for the designation as an

UNDERGRADUATE RESEARCH SCHOLAR

Approved by
Faculty Research Advisor: Dr. Jennifer Marshall

May 2023

Major: Physics

RESEARCH COMPLIANCE CERTIFICATION

Research activities involving the use of human subjects, vertebrate animals, and/or biohazards must be reviewed and approved by the appropriate Texas A&M University regulatory research committee (i.e., IRB, IACUC, IBC) before the activity can commence. This requirement applies to activities conducted at Texas A&M and to activities conducted at non-Texas A&M facilities or institutions. In both cases, students are responsible for working with the relevant Texas A&M research compliance program to ensure and document that all Texas A&M compliance obligations are met before the study begins.

I, Alexandra Boone, certify that all research compliance requirements related to this Undergraduate Research Scholars thesis have been addressed with my Faculty Research Advisor prior to the collection of any data used in this final thesis submission.

This project did not require approval from the Texas A&M University Research Compliance & Biosafety office.

TABLE OF CONTENTS

ABSTRACT

TOROS Camera Calibration

Alexandra Boone
Department of Physics & Astronomy
Texas A&M University

Faculty Research Advisor: Dr. Jennifer Marshall
Department of Physics & Astronomy
Texas A&M University

The Transient Optical Robotic Observatory of the South (TOROS) is a planned robotic observatory. The primary science goal of the observatory is to detect electromagnetic counterparts to gravitational wave phenomena. This project specifically focused on the characterization of the observatory's Charged Coupled Device (CCD). Several sets of bias and dark images were taken by the TOROS camera in 2020 and 2022 to test the CCD's dark current noise properties. These images were obtained and converted into .fits formatting using the CCD's proprietary software, ARCHONGUI. Python was then used to median combine the bias images into a master bias image. Several master dark images were generated, using images taken at multiple exposure times. The master bias image was then subtracted from each master dark image to create a "subtraction" image at each exposure time. The mean and median pixel values for each of the subtraction files were then plotted at each exposure time to measure the dark current noise output of the camera and ensure the instrument was working properly. The results using the 2020 images showed that the camera noise initially appeared to be within the factory expectations (13-30 Analog Digital Units (ADU)/pixel at 300s exposures), but the results using the 2022 images suggest the camera may need some additional testing prior to its shipment to Cerro Macón in Argentina.

DEDICATION

To everyone in the Physics Astronomy department at Texas A&M who supported me throughout my research process and academic journey..

ACKNOWLEDGMENTS

Contributors

I would like to thank my faculty advisor, Dr. Jennifer Marshall, and my project advisor, Dr. Ryan Oelkers, for their guidance and support throughout the course of this research.

Thanks also go to my friends and colleagues and the department faculty and staff for making my time at Texas A&M University a great experience.

The data and materials analyzed and used for TOROS Camera Calibration were provided by the TOROS team, including Ryan J. Oelkers, Luke Schmidt, Erika Cook, Darren DePoy, Mario Diaz, Lucas Macri, and Diego Garcia Lambas. The analyses depicted in TOROS Camera Calibration were conducted in part by Munnerlyn Astronomical Instrumentation Laboratory and these data are unpublished.

All other work conducted for the thesis was completed by the student independently.

Funding Sources

This work was supported in part by funding from the Texas A&M College of Science's Science Undergraduate Research Opportunities Program (SUROP).

NOMENCLATURE

TOROS	Transient Optical Robotic Observatory of the South
CCD	Charged Coupled Device
aLIGO	Advanced Laser Interferometer Gravitational wave Observatory (aLIGO)
GW	Gravitational Waves
EM	Electromagnetic
ADU	Analog Digital Unit

1. INTRODUCTION

1.1 Motivation

The observatory's primary science goal is to observe the electromagnetic counterparts to gravitational wave sources such as those discovered by the Advanced Laser Interferometer Gravitational wave Observatory (aLIGO) [1].

1.1.1 Gravitational Wave Astronomy

Gravitational Waves (GW) were only a theoretical prediction as recently as 50 years ago, based on the idea that mass and energy move in response to the curvature in space-time [2]. Gravitational waves are oscillations that propagate at the speed of light, replacing the previous Newtonian theory of gravity. They interact weakly with matter which allows them to propagate through space relatively undisturbed. The first evidence came from observations of a binary pulsar PSR 1913+16 by Russel Hulse and Joseph Taylor, who won the Nobel Prize for that work in 1993. Merger events occur when pairs of large objects come closer together until they coalesce and form a single compact object, which produces gravitational waves. Detecting gravitational waves requires that the sources are strong, such as those of merger events with large masses with large accelerations. Gravitational wave signals from neutron star and black hole merger events were already announced as detected by the Laser Interferometer Gravitational-Wave Observatory (LIGO) in 2015. LIGO utilizes three Michelson interferometers to detect gravitational waves in a large frequency and amplitude range. LIGO opened up the field to gravitational wave astronomy, showing that detection of these waves was indeed possible after Binary Black Hole mergers. LIGO was able to join with the Virgo observatory, creating a network of three interferometers, to detect several Binary Black Hole mergers since their initial detection, including events in December of 2015, and in January, June, and August of 2017. Using a system of three interferometers allowed for improvement upon the localization of the source [2]. In addition to black hole mergers, other astronomical events, which are among the most energetic in the universe, are expected to be observed using gravitational

wave detection. Such events include, but are not limited to, neutron-star-neutron-star (NS-NS) or neutron-star-black-hole (NS-BH) mergers [1].

1.1.2 Follow-up Observations

Events such as those NS-NS and NS-BH mergers are predicted to be some of the most energetic in the Universe. There have been an increasing number of candidates for these merger events, suggesting that detection of many more events will happen in the near future. These events are also predicted to have a variety of observable signals, including optical transients called macronova or kilonova. These are powered by radioactive decay of heavy nuclei synthesized in the merger through neutron capture [3]. It is additionally predicted that the emissions of these events will be mostly red and infrared. Observations of these transients that have been recently reported show signs that they follow the kilonova models, which indicates that the event could show that the mergers are the sources of short-hard gamma-ray bursts (SGRBs). One issue with gravitational wave detection is that they generally lack pointing accuracy which leads to large uncertainties in the target areas for electromagnetic follow-up observations. Therefore, wide-field cameras with the ability to do rapid follow-up observations are important to the detection of EM counterparts. The TOROS system was designed to provide these rapid follow-up observations of these signals in the optical spectrum.

1.1.3 Calibration

However, these optical counterparts may be faint, and their detection is limited to a large portion of the sky, so there may be large uncertainty in the measurement [4]. The calibration of the CCD system, particularly the dark current, needs to be ultra-precise to minimize the uncertainty in the measurement of these events.

The detector system includes a camera which has taken several dark and bias frames that are used to calibrate the noise produced by the instrument. Bias frames are images taken at a 0 second exposure time with the camera shutter closed. This is used to determine the noise created by the instrument itself. Dark frames are frames taken at exposure times matching those of the light

frames, but with the shutter closed. The dark current frames measure both the noise produced by the instrument and noise produced by heat generated when the camera takes images at different exposure times. The noise generated by the heat is called dark current noise, which is what was found in this project. Dark current noise output is measured to ensure the camera works properly to take data at several exposure times. Data collected from recent images is compared to data collected almost two years prior, when the detector was being initially developed before the project was put on pause due to the COVID-19 pandemic. The data collected is reduced using a code developed in Python to calculate the expected dark current noise output of the camera and has ensured that the detector is in proper working condition before it will be shipped to Argentina.

Other methods of calibration include taking flat field images, or images are images taken with a uniform brightness, usually taken of a lit up wall or a clear sky. These images are used to correct irregularities in pixel values by measuring each pixel value and comparing it to the mean pixel value. Ideally, each pixel should respond to the same photon flux (light) in the same way. However, it is normal to have variations. These variations are called the photon transfer curve (PTC) [5] of the sensor. Flat field images taken at different exposure times can also be used to demonstrate the linearity of the device, as the longer exposure times should show an increase in signal. Using flat field correction methods is ultimately meant to remove that variation in sensitivity from pixel to pixel, and using flat field testing can reveal more characteristics of the device. Wavelength filters can also be utilized for calibration of the wavelength range of the detector. Wavelength range refers to the range of wavelengths the CCD can detect. The filters have a different throughput, or amount of flux which can pass through. Taking images at varying exposure levels using each filter can allow for the testing of the CCD's noise properties over many wavelengths [6].

1.2 Background

1.2.1 TOROS Characteristics

The TOROS detector system is a robotic optical observatory currently under construction in Northern Argentina with first light expected in mid 2023 [4]. The observatory provides a large

field-of-view to more effectively search the celestial sphere for sudden changes in brightness, also known as transients. TOROS has a field of view of 9.85 square degrees and has a broad bandpass of around 0.4 -0.9 μm. TOROS is designed to be fully robotic and will have modes of operation including the follow-up of gravitational-wave triggers, follow-up of γ ray burst triggers, baseline imaging of surveyable areas, and search for transient events, variable sources, and moving objects within the fields from Dark Energy Survey (DES) and VISTA-VIKINGS, which is a European Southern Observatory survey. The main goal of TOROS is to maximize the chance of detecting electromagnetic counterparts to gravitational wave events like neutron star-neutron star or neutron star-black hole mergers. TOROS will take 15 minute exposures for 7 hours on an area localized by a two and three interferometer coincident scenario developed by Kasliwal and Nissanke [7]. TOROS hopes this will lead to finding coordinates of those follow-up events.

1.2.2 Charged Coupled Devices

The TOROS detector system includes a Charged Coupled Device (CCD) that this project is focused on characterizing. CCDs were invented in the 1960's and were originally created to work as a new type of computer memory circuits. However, their potential for imaging was soon understood, and CCDs started to be used more for that purpose. CCDs are made up of a semiconductor which is composed of smaller cells called picture elements (pixels), an overlying dielectric film, and a conductive gate. CCDs are compact and sensitive, and have a linear response to the detection of light. CCDs also have a wide range of detection capabilities which allows them to respond well to both brighter and fainter objects. These CCDs are individually characterized by their linearity, quantum efficiency, and gain and noise levels [8]. CCDs have many types, including front-illuminated and back-illuminated, which refers to the way photons are able to travel to the detectors. In general, back-illuminated CCDs have a higher quantum efficiency and allow for better detection of bluer photons [9]. Quantum efficiency describes the ability to convert photons to photoelectrons. The photons are the light particles that hit the camera, and the photoelectrons are collected by the CCD for readout. Noise in many imaging devices is produced largely by photon shot noise, which is due to the random detection of photons. The circuit used by the CCD, however, also contributes to

noise. This sets the minimum noise the device will read [8]. Noise can be reduced by cooling down CCDs. There are a few ways to do this, but they must also ensure that the cooling method doesn't leave the CCD susceptible to moisture from condensation. Some techniques used commonly to cool down CCDs include liquid nitrogen or cryo-coolers. However, these must be accompanied by a vacuum to seal the CCD so moisture is less likely to form. This technology works by connecting a vacuum chamber with the detector in it to a vacuum pump to pump out the air. Vacuum pump technology is utilized in TOROS and so pumping down the air in the detector and cooling down the system is a necessary first step when using the CCD. Limitations to CCDs include static distortions, which occur due to the physical geometric imperfections of the CCD. Other limitations include bad pixels, columns, or rows, which are unable to detect flux, and "tree ring" patterns, which are concentric discrepancies in the detection of flux that can be observed through taking flat field images. These limitations are often due to the physical properties of the device, and are usually linked to the way they are manufactured [6]. Overall, CCDs are becoming more and more efficient as manufacturing technologies improve and they have many great properties which make them a sensible and attractive choice for astronomical observing purposes. The TOROS CCD is called STA1600LN, which is back-illuminated for higher sensitivity. It has a 1560 x 1560 image element with pixel spacing of $9\mu m$ x $9\mu m$ and has a readout Noise of 2e$-$ at 50 kHz and 5e$-$ at 1 MHz [10].

1.3 OAUNI Project

Many astronomical surveys characterize their detectors in a similar fashion [11]. One such survey, detailing the Astronomical Observatory of the National University of Engineering (OAUNI) Project, showed a similar characterization of CCD detectors which will give an example on how this project was completed and provides a frame of reference in which to compare our results to. This paper measured the gain and readout noise for another CCD detector, which is part of a camera called SBIG STXL6303E. It will be used at UNI astronomical observatory. The project is located in Huancayo in the Peruvian Andes, and is aimed at developing teaching and outreach programs in the field of astronomy. To obtain precise calibrations of the camera, systematic tests

can be done. The project, like ours, consisted of measurements taken in the form of dark current images and bias images, but also included flat field images. Flat field images are used to note the linearity and gain of the camera. These images are taken with a homogeneous illumination, and in this case it was done by shining a white LED on the roof of the lab. What differs from our project is the flat field images and that they were taken at a fixed temperature of $-5°$C. The dark current images were taken at exposure times of 0.4, 1, 2, 3, 5, 8, 11, and 14 seconds. The images were reduced in the Image Reduction and Analysis Facility, IRAF, a software designed for reducing astronomical data. The flat field and dark images were first corrected by subtracting the mean value of the overscan region for each individual image. This method of using the overscan region is intended for selecting the optimal region for data. This was necessary in this project since the constraints of the device required the bias frames to be taken at a 0.4s exposure time rather than a 0 second exposure time. This overscan corrected the 0.4s exposure time bias images to be as close to a zero second exposure as possible so it could be representative of the zero bias images. The mean was taken of the bias, dark, and flat field images, at each exposure time, and the mean of the bias images were used to subtract off the flat field and dark images to "correct" them. This allowed the dark images to show only the temperature component of the noise. This is the same process that was done in this TOROS camera calibration. A difference in this project, however, is the usage of the flat field images. These images were used to measure the gain and were corrected by the dark images to observe the effects of the dark current noise on gain output. The results showed that the flat field images showed a range of gain that was within the expectations of the device, around 1.47 e$-$/ADU. The flat fields corrected with the dark current showed that dark current had a negligible effect on the device properties, indicating that data could be reduced using overscan and bias correction alone. Readout noise was calculated from the dark current images, without overscan correction. The results indicated that the mean readout noise showed a small dispersion and was very precise. The gain and readout noise levels were found to be 1.654 ± 0.012 e$-$/ADU and 12.2 e$-$, respectively. This was compared with the readout noise and gain provided by the manufacturer, and it was found that the results were in general agreement with the nominal values

for the detector, with only a slightly elevated value of around 11-12% [11].

2. METHODS

The bulk of this project was divided into three main tasks. The first task was converting the images taken by the TOROS camera into .fits formatting using its proprietary software, which was necessary to extrapolate the data needed from them. The next step was combining the sets of images into master bias and master dark files, and then creating individual subtraction files from those master files for each exposure time the dark image captured. The final step was to reduce the data from those files to find the mean and median values, which allowed for making meaningful observations about the characteristics of the noise properties of the camera. The methodology for each step of the project will be detailed below.

2.1 Converting the Images

The first step of the project was getting the images converted into .fits formatting from the .raw format they were in when the images were initially received. The images included both dark and bias images, which are used to calibrate the noise output of the camera. Bias images are taken with the shutter closed at a 0 second exposure time, while dark images are taken with the shutter closed at several different exposure times which will match the exposure time of the light images. While there are methods available to convert the images using Python or other coding languages, it was the fastest to convert the images manually in the CCD's proprietary software, which is called ARCHONGUI. This software system is intended for reducing astronomical data from the specific device. This was done on the computer available in the Munnerlyn Astronomical Instrumentation Laboratory. The images were available in a shared Google Drive for the TOROS project, and in ARCHONGUI the images could be easily imported from that drive and re-saved in the proper formatting. Each image was imported from the drive, opened in ARCHONGUI, and re-named and re-saved in a folder. After all the images had been converted, the folder was moved back into the shared drive so the data would be easily retrievable.

2.2 Combining the Files

The next part of the project was to combine the files into master files. The bias images needed to be combined using a median of each of the bias images into a single master bias file to ensure the most accurate representation of the noise level. The master bias file is used to measure the dark fixed-pattern noise, or the noise produced by the instrument itself. Noise also occurs from dark current, which comes from heat produced by the instrument. The dark current noise can vary by exposure time, so it was necessary to have several sets of dark images taken at different exposure times. Each set of dark images were combined using a median in a similar fashion to the bias image to obtain several master dark files at each exposure time. Once the files were combined, the dark current at each exposure time could be found by subtracting the bias image noise from the dark image noise at each exposure time. This was done in Python. The bias images were done first. Astropy and Matplotlib were used to create a data cube of each of the images. The median of the data cube was then found to provide the final combined image. This median was then saved to its own .fits file, which is called the master bias file. The same process was done for the dark images. Master dark files were created using a median combination for data cubes at each individual exposure time, meaning that each exposure time got its own master dark file. The files were then saved individually as .fits files according to exposure time. The final step was to create individual subtraction files to measure the expected dark current noise output of the camera. These subtraction files were created by subtracting the master bias file from each of the individual master dark files. The subtraction files were created using Python, by subtracting the median bias value from each of the median dark values. The subtraction files were then saved as .fits files using Python so they could later be used. This essentially subtracted the noise due to the instrument and the heat from the noise produced by the instrument, leaving only the thermal noise. This process was done for the images initially taken in 2020 and again for the images taken in 2022.

2.3 Reducing the Data

The final step of the project was to reduce the data found from the dark current noise output. The noise level at each exposure time was reduced by taking the mean and median. These values

were found using Python code. The mean and median values found at each exposure time were then individually plotted in Python using Matplotlib to find any abnormalities in the camera at certain exposure time. This process was repeated for both the images initially taken by the camera, and the more recent images taken by the camera. The dark current noise median and mean plots were compared for both sets of images to ensure that the camera was still working properly after its period of disuse.

3. RESULTS

The results of this project are divided into the results from the 2020 images and the 2022 images, and a comparison of the two.

3.1 First Set of Images

The results of the measured noise levels at each exposure time for the 2020 images were put into two graphs for better visualization of the data. These figures, which show the mean and median values of that noise, are shown below.

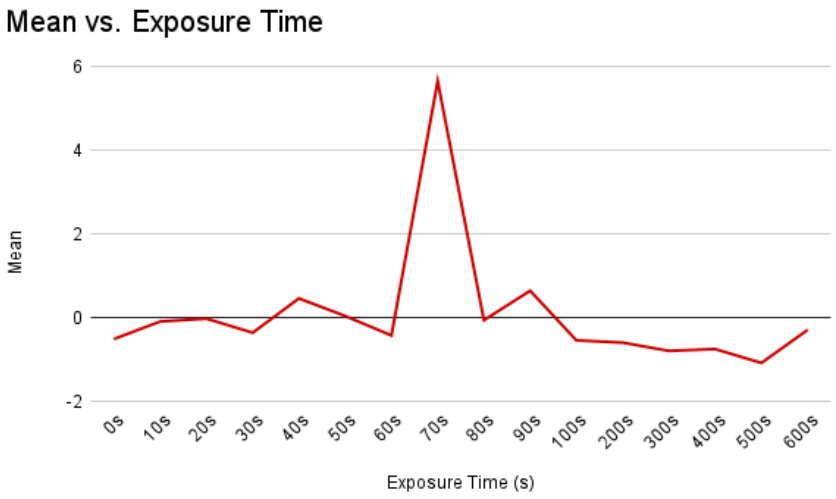

Figure 1: *Mean Values (counts) vs. Exposure Time (s) for 2020 Images*

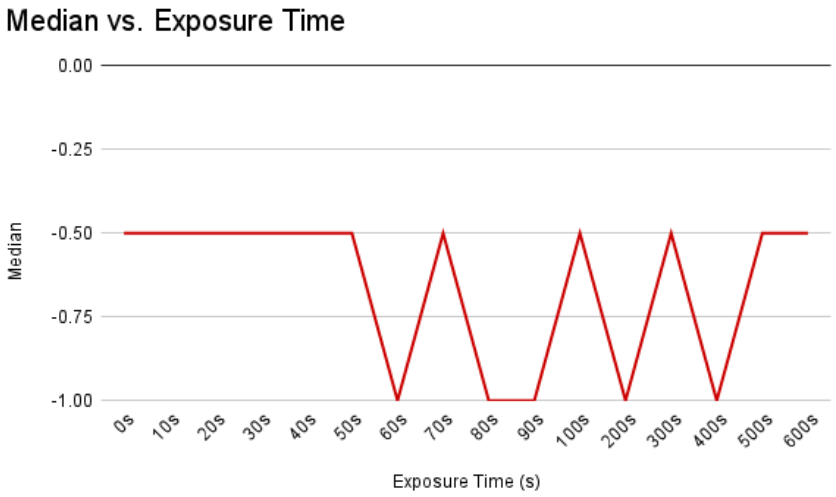

Figure 2: *Median Values (counts) vs. Exposure Time (s) for 2020 Images*

The first set of images yielded dark current noise output mean values that were close to 0, with only a slight deviation from this in the 70s exposure time images. The mean graph doesn't show much of one solid trend, as the most notable feature is that spike of a higher mean value. However, although the spike is notable in the figure, compared to the standard deviation, the higher mean value is likely negligible for our purposes. Although the trend in the median graph can be seen to bounce up and down, it should be noted that the values all remain between -0.5 and -1. The median values similarly stayed flat and hovered close to 0 for each of the exposure times. The mean values also remained constant for the most part, with the exception of that one exposure time which had shown the slightly elevated mean value. Overall, however, this data shows that the noise level found in the first set of images were within the expected constraints of the device. Although longer exposure times are usually correlated with noise levels, those longer exposure times should still stay within the constraints, which is what was found in the initial set of data.

In summary, the results from the mean and median values obtained by the subtraction files obtained from the first set of images show that the noise output read from the 2020 images are well within the factory's expected constraints of the instrument. The trends of the mean and median values did not show a correlation of noise with exposure time, which can be expected, as the higher

exposure times generate more heat. Despite this, the mean and median values stayed close to 0, which is what should be expected at these exposure times, since the device had a proposed measured dark current of 0.0004e−/px/s. The main abnormality in the data was that the 70s exposure time showed a heightened mean value, which may need to be further looked into. Several things could have caused that elevated noise level in those images. Ultimately, however, the difference in 5 or 6 counts should be negligible to producing the results TOROS will obtain. The results found from these images indicate that the dark current noise from the camera was properly calibrated in 2020 to precise levels.

3.2 Recent Images

Similarly, the mean and median values of the dark current noise output of the second set of images were plotted, and these figures are shown below.

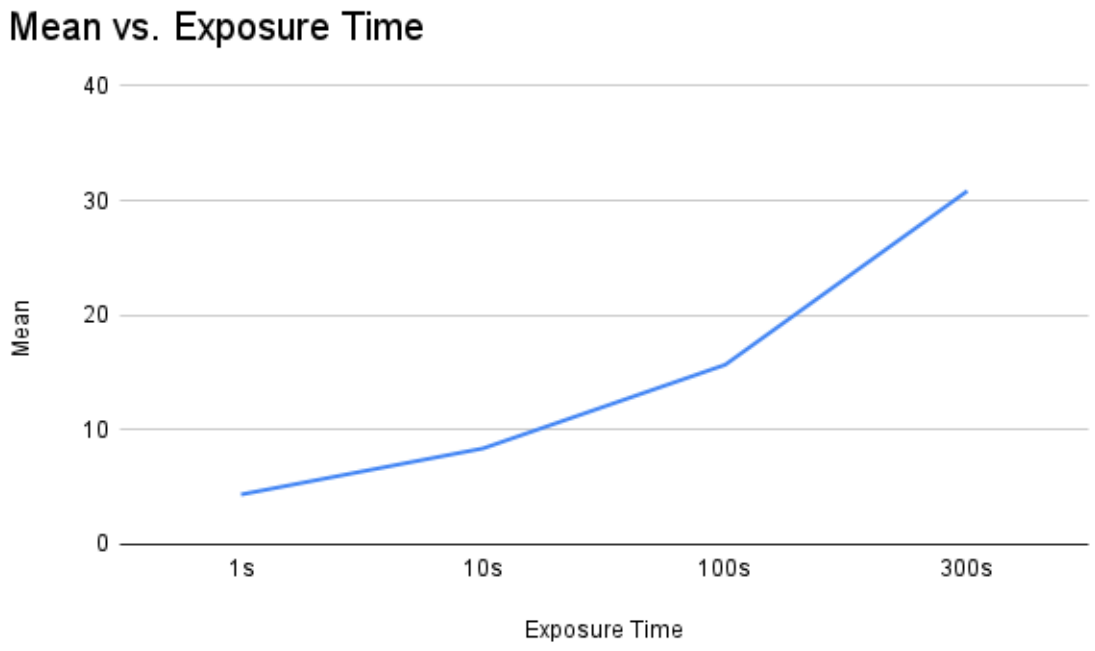

Figure 3: *Mean Values (counts) vs. Exposure Time (s) for 2022 Images*

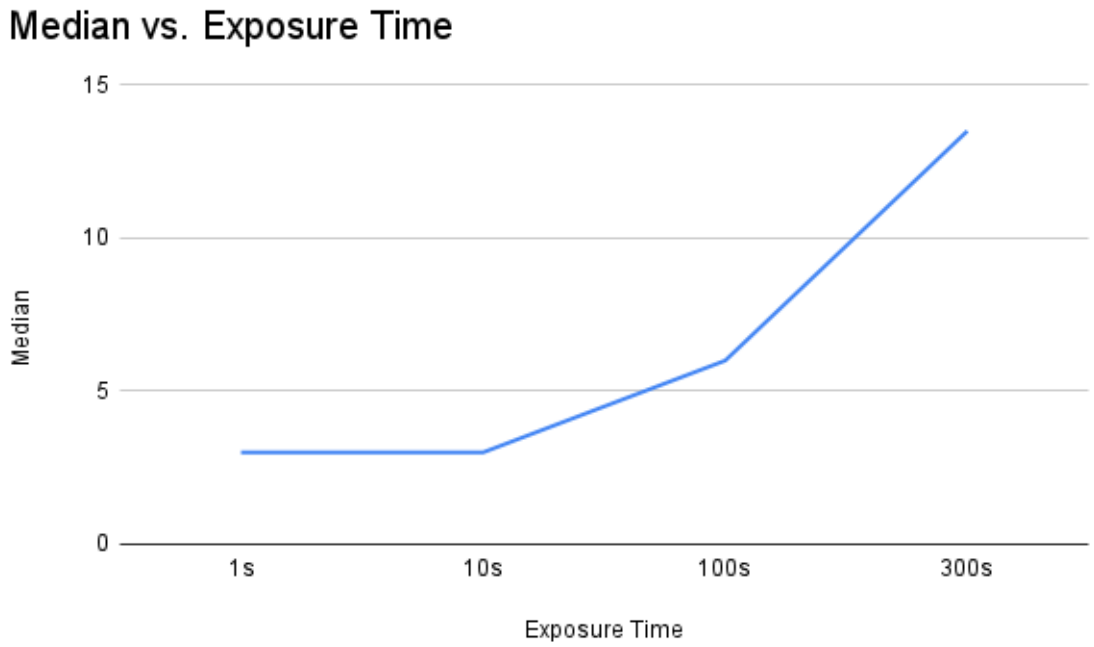

Figure 4: *Median Values (counts) vs. Exposure Time (s) for 2022 Images*

This second set of images showed an upward trend in the noise level with exposure time in both the mean and median graphs. Although the trend was the same for both the median and mean graphs, the noise levels measured in the mean was much higher than that of the first images. This was seen at each exposure time. The mean, for example, showed a noise output of 30 counts per pixel, or about 75e− per pixel at the highest exposure time, while the median value peaks out at around 12 counts per pixel. Reasons for this discrepancy will be addressed to note whether it could affect TOROS results. In summary, the results from the recent images show a trend in noise that is to be expected, since longer exposure times generate more heat, and therefore more noise. However, the value of the dark current noise output was much higher than what was expected at that exposure time from the device. It can be noted that the mean levels were higher than that of the median. This could indicate that there were a few outliers, pixels with higher noise levels that dragged up the average. These outliers may still be important to note in the calibration of the camera. One possible source of the elevated noise could be a possible light leak when taking the

images. The frames are meant to be taken in complete darkness, when the shutter is closed, but the room had some LED lights on whose light could have reached the detector and caused an inflated noise level to be measured.

3.3 Comparison

The older images showed a different result than the most recent ones. Although the recent (2022) images showed a trend more as expected by the camera, the older images (2020) are more within the constraints set about by the factory for the device. As mentioned previously, further testing will have to be done to see what caused such a large discrepancy between the sets of images. The elevated noise levels in these newer images could indicate a light leak with those images. This could happen because the room where the camera took the images was not completely dark, as some small LEDs were still turned on, although the camera shutter was closed and covered. Although this is a possibility, further testing will need to be completed to verify or nullify that.

3.4 Implications

In summary, this project was aimed at testing the CCD's noise properties, focusing specifically on the dark current noise output of the camera. The device has an expected measured dark current of about 0.0004e−/px/s, and whether or not the measured values of the noise properly fit into those constraints would indicate if the device is functioning well. Several sets of dark and bias images were taken in 2020 and 2021, and comparing the results obtained can tell us if the noise from the camera was well constrained in 2020 and if it is still functioning as it was previously. The images from 2020 ended up showing a flatter trend with exposure time, and indicated well-constrained noise levels that were within the expected properties of the device. The 2022 images, however, showed an upward trend of noise with exposure time. This trend is common when measuring the dark current noise of CCD's, as longer exposure times require the camera to be on for longer and heats them up more. However, the noise level was higher than the expected constraints of the device. The expected noise output for a 300s exposure time, for example, is around 0.12 e− per pixel, while the results from the 2022 images showed a level of 75 e− per pixel. Clearly, there is

a discrepancy to be addressed. Although the noise level was only slightly higher than what should be expected, this indicates that there may be an issue with the images or possibly an issue with the CCD. One possible reason for this discrepancy includes a light leak when the images were taken. The images are meant to be taken in complete darkness, but since there were windows in the room the CCD was in, it is possible some light was allowed through and shone on the CCD. This would cause an elevated noise level as the camera was detecting those photons and giving a response. Another possibility could be the camera was not properly cooled and vacuum sealed, leading to an increased noise level reading from the CCD. The multiple possible causes of this discrepancy means that further testing will have to be done to ensure that the issue is with another outside cause and not with the CCD itself.

4. CONCLUSION

The results found in this project were analyzed in two parts, the 2020 images and the 2022 images. Then they are compared to indicate whether the properties of the device have changed significantly between the two sets of images. Additionally, next steps in characterizing the device will be explored and detailed.

4.1 Future Research

Overall, this project was aimed at characterizing the dark noise current output of the Charged Coupled Device of the TOROS detector system. Although the noise levels measured in the first step of the project generally are in agreement with the constraints set forth by the factory for the device, the second set of images indicate further testing should be done to ensure the device is operating within the factory restraints on the device. Additionally, further testing of the device could certainly be done to further characterize the detector and ensure it is still functioning up to the factory's standards. Some of the further research that could be done will be discussed below.

4.1.1 Re-taking Images

Next steps with the project will largely be with addressing the issue found with the 2022 images. The first step could be retaking photos and ensuring the room is completely dark. This step could have been completed prior to finishing this project, but a new vacuum pump was needed to cool and vacuum seal the detector that was not yet available by the end of the project. If the reduction of those images show a result closer to that of the factory expectations, it can be assumed that the heightened noise level was due to a light leak in those images. This will be the next step in ensuring the camera is still properly calibrated. If the images still show that elevated noise level, further troubleshooting may need to be done to see what the issue could be.

4.1.2 Flat Field Imaging

After addressing this primary issue, another step in characterizing this CCD could be to make linearity and photon transfer curves for the device based on new testing. This can be done using flat field images, such as those described previously in the OAUNI project. Reducing data collected from these images could allow for further calibration of the gain of the camera. Linearity and photon transfer curves have already been created for the device, so recreating the curves based on new flat field imaging and comparing them to the previously created trend lines can serve as a test of its performance. The flat field images could also be utilized for calibration of the wavelength range of the detector. This would characterize the CCD's noise properties over a range of wavelengths, and would show if the CCD functions well over each wavelength, and which wavelengths the CCD is best suited for. It will also allow for testing to find the ceiling of the wavelength range, or the faintest object at which the CCD can no longer detect photons.

4.1.3 Auto-Focus System

Another step that could be included in characterizing the TOROS CCD could be developing an auto-focus system. Focusing could be calibrated by taking multiple exposures and varying the distance from the detector to calculate the focus position. This could be done by plotting the image contrast, or the ratio of intensity in the brightest pixel to the total intensity of the focus range, as a function of the distance of the image from the camera. The maximum of the curve will then give the correct focus position [6]. Once this is found, the function can be implemented into the main software of the device so the device can find the focus position and place itself at it automatically.

4.1.4 Knife Edge Scan

One more test that could be done on the CCD is a knife edge scan. Knife edge scans uses several low resolution images of a signal and tries to recover an image of the signal with better resolution. This is done by progressively shifting the low resolution image behind a barrier in steps, only allowing light to transmit on one side of the barrier. This tests how the signal is resolved at each step. Knife scans can be material, or virtual, which uses an edge that causes no light scattering.

The goal of this kind of scan is to test the charge diffusion qualities of the CCD to measure the Point Spread Function (PSF) of the CCD. The scans use the steps to scan the signal and use a basic image processing procedure to estimate the background of the signal. This process includes taking the median flux of the pixels to evaluate the pedestal, estimating readout noise from the standard deviation of the pixel flux, subtracting the pedestal, taking the median again, and finally computing the shift of the signal [6]. Python can be utilized to carry out this kind of scan and background estimation as well as the data reduction that goes with it, and the results will be able to show the diffusion width parameter of the CCD, which could be compared to results on similar sensors to ensure the measurements indicate an appropriate PSF for our device.

4.2 Summary

In summary, the TOROS CCD will soon be shipped to Cerro Macón in Argentina where it is commissioned in the TOROS observatory. The same dark current noise calibration done in this project will be repeated on the CCD after its arrival in Argentina to assure the device is still functioning properly after shipping. The measurements done in this project will serve as an important baseline for the quality of the CCD after its permanent installation.

REFERENCES

[1] J. A. et al., "LIGO Scientific and Virgo Collaborations," 2010.

[2] B. P. A. et. al., "Ligo: The laser interferometer gravitational-wave observatory," 2009.

[3] L. X. Li and B. Paczynski 2013.

[4] M. D. et. al, "The TOROS Project," pp. 225–229, 2020.

[5] P. A. et. al., "The Shape of the Photon Transfer Curve of CCD Sensors," 2019.

[6] N. Petitdidier, "LSST: Characterization of the CCD sensors," 2015.

[7] S. N. et. al. 2013.

[8] B. E. B. et. al., "CCD Imager Development for Astronomy," pp. 393–412, 2007.

[9] F. WK, "Digital Imaging Techniques," pp. 189–212, 1979.

[10] I. Semiconductor Technology Associates, "STA1600LN Test Report," 2023.

[11] A. P. et al., "Characterizing a CCD detector for astronomical purposes: OAUNI Project," 2016.